Remote Sounding of Cloudy Atmospheres. III. Experimental Verifications

M. T. CHAHINE, H. H. AUMANN AND F. W. TAYLOR

Jet Propulsion Laboratory, California Institute of Technology, Pasadena 91103

(Manuscript received 29 July 1976, in revised form 7 December 1976)

ABSTRACT

The cloud-filtering technique developed in Parts I and II of this study is experimentally verified in this paper. The verification is based on radiance data measured in the 4.3 and 15 μm CO_2 bands using a multidetector sounder mounted on an aircraft. The results presented here show that, from the aircraft height of 7.6 km and in the presence of multiple cloud formations, it is possible to recover simultaneously:

1) The clear-column atmospheric temperature profile with an rms error of 1 K with respect to radiosondes.
2) The land and sea surface temperature at all sun zenith angles. The accuracy of the recovered sea-surface temperature is 0.5–1 K with respect to measured bucket temperatures.
3) The humidity profile (water vapor mixing ratio) with a precision of 10%.
4) The fractional covers and heights of up to three cloud formations.
5) The types of clouds, i.e., whether convective or nonconvective.

1. Introduction

This is the last of three papers dealing with the problem of infrared remote sensing in the presence of clouds. In the first two papers (Chahine, 1974, 1976) an analytical method was derived for the determination of clear-column atmospheric parameters from radiance data measured in the presence of clouds. According to this method the effect of clouds is eliminated analytically by considering observations in adjacent fields of view and in two different wavelength regions of the spectrum.

Specifically, in Part II we express the effects of multiple cloud formations on the outgoing radiance as a function of the fractional cloud cover in each field of view and as a function of the radiative transfer properties of the clouds. We proceed then to eliminate all terms containing the optical properties by considering measurements in adjacent fields of view. In the resulting system of nonlinear integral equations the ratios of the fractional cloud covers (defined as cloud coefficients) and the clear-column vertical temperature profile are essentially the only remaining unknowns. The solution of this system of equations is carried out simultaneously by interations as described in Part II. According to this iteration scheme we use the shorter wavelength radiance data to determine the clear-column temperature profile and the longer wavelength data to determine the cloud coefficients. These coefficients are independent of frequency and can, therefore, be used to reconstruct the clear-column radiance for any sounding frequency which observed the same clouds.

Several numerical tests, using simulated clouds and radiance data, were carried out in Parts I and II to demonstrate the validity of this cloud-filtering approach. In this paper, however, we verify the method under real atmospheric and cloud conditions using field measurements of the outgoing radiance corresponding to the set of sounding frequencies shown in Table 1.

To this end a multidetector grating spectrometer, capable of measuring the outgoing radiance *simultaneously* in all sounding channels, was constructed and flown on an aircraft. Details of the instrument

TABLE 1. The set of sounding frequencies for the aircraft-mounted sounder and their primary objectives.

CHANNELS	FREQUENCIES	OBJECTIVES
1	2660 cm^{-1}	SURFACE TEMPERATURE (DAY AND NIGHT)
2	2601	
3	2517	
4	2298	ATMOSPHERIC TEMPERATURE PROFILE
5	2281	
6	2260	
7	2241	
8	2222	
9	2203	
10	2187	
11	2170	
12	1885	WATER VAPOR PROFILE
13	1863	
14	1843	
15	900	SURFACE TEMPERATURE
16	773	CLOUDS EFFECTS
17	744	
18	726	

design and calibration are described elsewhere by Aumann and Chahine (1976). The multidetector approach is necessary here in order to ensure that all the sounding frequencies observe the same clouds at the same time.

The aircraft measurements were taken from a height of 7.6 km over the Gulf of Mexico and its shore and were repeated for different sun angles and under various clouds and surface conditions as described in Section 2. In Section 3 we analyze the data and describe the basic steps needed to recover the clear-column temperature profiles, the surface temperature of the ocean and the solid earth, the water vapor mixing ratio and the heights, amounts and types of clouds in each field of view. The results are illustrated in Section 4 and compared with available *in situ* measurements.

2. The aircraft observations

Five separate flights of the multidetector instrument were carried out on the NASA-P3A aircraft during the month of July 1975. The flights were made over the Gulf of Mexico and its surroundings under different sun angles and types of clouds. Photographs of the fields of view were made during the flights, and observers on the plane made visual estimates of the types, amounts and heights of the clouds.

A list of the sounding frequencies is given in Table 1 with a description of their primary functions. The spectral resolving power is 1% for the first 15 detectors and 2% for the remaining ones. The experimental signal-to-noise ratio was in excess of 100:1 for the first 15 detectors and ranged between 100:1 and 40:1 for the remaining channels. Additional details related to the instrument performance are given separately by Aumann and Chahine (1976).

During the instrument flights each sequence of observations consisted of five blackbody calibrations interspaced with four earth radiance measurements, carried out simultaneously for all channels. We recall here that the cloud-filtering method derived in Part II requires measurements in four adjacent (or consecutive) fields of view in order to eliminate the effects of multiple cloud formations. The geographical locations of every other set of these measurements is shown in Figs. 1–3. The size of each field of view is 2.5 km $\times$3.0 km from the aircraft height of 7.6 km.

The first flight was intended to check the calibration of the instrument and the accuracy of the computed atmospheric transmission functions. During the flight the aircraft passed over the radiosonde station at Lake Charles, La., then flew over the Gulf of Mexico to a point near 27°N, 92°W. The southward flight was made at an elevation of 0.3 km above the ocean and the return flight was made along essentially the same path, at an elevation of 7.3 km. The clear atmospheric conditions below 0.3 km together with the low atmospheric attenuation from this low height ($0.98<\tau<0.99$) allowed us to recover a surface *brightness* temperature of 301.5±0.5 K from all of the temperature sounding channels, except the strongly absorbing frequencies such as 2298 and 2281 cm^{-1}. The brightness temperature $\tilde{T}$ is defined by

$$B(\nu_j,\tilde{T})=\tilde{I}(\nu_j), \tag{1}$$

where B is the Planck function and $\tilde{I}(\nu_j)$ the radiance measured at frequency ν_j. Considering that the atmosphere is not perfectly transparent, the values of the recovered brightness temperature from the low-altitude flight were in good agreement with the average bucket temperature of 302.17 K measured at 27°26.0′N, 91°47.5′W by an ocean research vessel operated by Texas A & M University.[1]

We analyzed the data from the 7.3 km altitude flight, then compared the recovered surface temperature with the brightness temperature obtained from the low-altitude flight and compared the recovered clear-column atmospheric temperature profiles with the profile measured by the radiosonde station at Lake Charles. In all cases the agreement was within 1 K. Consequently, we concluded that the accuracy of the instrument and its calibrations are acceptable. We assumed, however, that all systematic discrepancies between the recovered and radiosonde temperature values are attributable to minor errors in the computed atmospheric transmission functions. These functions were computed on the basis of McClatchey (1973) spectral line data.

To "improve" the accuracy of the computed transmission functions $\tau_{\text{computed}}(\nu,p)$, we applied the tuning technique developed by Jastrow and Halem (1973) in which

$$\tau(\nu,p)\,|_{\text{adjusted}}=[\tau_{\text{computed}}(\nu,p)]^{1+e(\nu)} \tag{2}$$

and determined the values of $e(\nu_j)$ which gave the best agreement between the measured and recovered temperature values. The resulting values of $e(\nu_j)$ were very small and ranged between

$$-0.05\leqslant e(\nu_j)\leqslant 0.01 \tag{3}$$

for all the sounding frequencies. We applied the values of $e(\nu_j)$ obtained from this flight to adjust the computed transmission functions for all subsequent flights, even though the remaining flights were made at a slightly higher altitude.

The following three flights consisted of one morning and two afternoon flights made at an elevation of 7.6 km (~390 mb). During these flights the aircraft flew over areas ranging from clear to extensive cloudiness with different cloud types ranging from low haze to high cumulus. During the last flight the aircraft

[1] Private communication, Professor William M. Sackett, Texas A & M University.

encountered very high clouds and was not able to fly above them. The data returned from this flight were not suitable for the purposes of this paper.

3. Data analysis methods

The numerical techniques needed to analyze the measured radiance data have been described in detail in Parts I and II and in earlier papers by Chahine (1968, 1970, 1972) and by Shaw (1970). The objective in this section is to formulate the basic equations for the case of this experiment and to outline the main steps followed in analyzing the data.

The fundamental equation used throughout this section describes the relationship between the clear-column radiance $\bar{I}(\nu)$ and the radiances $\tilde{I}_k(\nu)$ measured over adjacent fields of view (subscript k) as

$$\bar{I}(\nu)=\tilde{I}_1(\nu)+\eta_1[\tilde{I}_1(\nu)-\tilde{I}_2(\nu)]+\eta_2[\tilde{I}_1(\nu)-\tilde{I}_3(\nu)]+\eta_3[\tilde{I}_1(\nu)-\tilde{I}_4(\nu)]. \quad (4)$$

Eq. (4) was derived in Part II to eliminate the effects of up to three cloud formations using radiance data measured over four *adjacent* fields of view. In this experiment, however, we will take $\tilde{I}_k(\nu)$ from measurements over four *consecutive* fields of view along the path of the aircraft. The cloud coefficients η are independent of frequency and their value, at this stage, remains to be determined.

The clear-column radiance $\bar{I}(\nu)$ in Eq. (4) is related to the clear-column atmospheric temperature profile through the radiative transfer equation, for a plane parallel and homogeneous atmosphere, by

$$I(\nu)=B[\nu,T(p_s)]\tau(\nu,p_s)+\int_{\ln p_s}^{\ln \bar{p}} B[\nu,T(p)]\frac{\partial \tau(\nu,p)}{\partial \ln p}d\ln p, \quad (5)$$

where B is the Planck function,

$$B(\nu,T)=a\nu^3/(e^{-b\nu/T}-1), \quad (6)$$

and $\tau(\nu,p)$ is the transmittance of a clear-column of absorbers between pressure level p and the aircraft level $\bar{p}$.

Eqs. (4) and (5) are solved simultaneously by iteration to recover the clear-column temperature profile under the instrument and to determine the values of the cloud coefficients η_l.

a. The clear-column temperature profiles

The clear-column atmospheric temperature profiles $T(p)$ are derived from the set of 4.3 μm channels between 2298 and 2187 cm^{-1}, while the cloud coefficients η_l are evaluated from the set of 15 μm channels between 773 and 726 cm^{-1}. The determinations of $T(p)$ and η_l are obtained simultaneously according to the method described in Part II. We started our iterative solutions with an isothermal initial guess for the temperature profile, $T^{(0)}(p)=$ constant, and used a linear interpolation formula for quadrature purposes. We found the rate of convergence to be relatively slow and the solution took 10 iterations to converge. This slow rate of convergence is due to the fact that the weighting functions, $\partial\tau/\partial \ln p$, tend to become very broad for observations made from low altitudes, as in the case of this experiment (the only exceptions are the two sounding frequencies 2298 and 2281 cm^{-1} located near the center of the 4.3 μm CO_2 band). This unfavorable property of the weighting functions becomes less severe, however, in the case of observation from satellites or high-altitude balloons.

Since the cloud coefficients are independent of frequency we will take the values of η_1, η_2 and η_3 derived here to reconstruct the clear-column radiances for the entire set of sounding frequencies given in Table 1. From here on we can deal directly with the clear-column radiance values for the recovery of the water vapor profile and the surface temperature.

b. The water vapor mixing ratio

The clear-column water vapor mixing ratio $q_{H_2O}(p)$ is obtained from the set of radiance data measured in the 6.3 μm band between 1885 and 1843 cm^{-1}. The solution for $q_{H_2O}(p)$ is obtained according to the method derived by Chahine (1972) in which Eq. (5) is integrated by parts and written in the form

$$\bar{I}(\nu)=B[\nu,T(\bar{p})]-\int_{\ln p_s}^{\ln \bar{p}} \tau[\nu,q_{H_2O}(p),\ldots]\frac{\partial B[\nu,T(p)]}{\partial \ln p}d\ln p \quad (7)$$

where $\bar{I}(\nu)$ is the clear-column radiance reconstructed from Eq. (4) using the three cloud coefficients η_l derived earlier, and $T(p)$ is the clear-column temperature profile. The solution for $q_{H_2O}(p)$ is obtained by iteration starting with $q^{(0)}_{H_2O}(p)=10p^{2.5}$ and using linear interpolation on a $\ln p \times \ln q$ scale for the recomputations of $\tau^{(n)}[\nu, q^{(n)}_{H_2O}(p), \ldots]$. The rate of convergence in the case of this experiment was moderate and uniform and the solution was terminated after six iterations.

c. The surface temperature

The surface temperature T_s of the ocean and solid earth can be derived from the radiance data measured in the 3.7 μm transparent region between 2660 and 2517 cm^{-1} as well as from the 11 μm water vapor continuum at 900 cm^{-1}. The effects on the accuracy of the recovered values of T_s of surface emissivity, reflection of solar radiation and variations in the concentration of water vapor in the atmosphere are different in the two bands. In the following analysis

we will discuss the accuracy of the surface temperature derived from each of these two transparent regions.

1) THE 3.7 μm CHANNELS

During daytime the earth's surface may scatter solar radiation and thus the clear-column radiance $\bar{I}(\nu)$ of Eq. (4) becomes a function of the reflected solar radiation as well as the thermal radiation from the surface and the atmosphere. In this case, Shaw (1970) modified the right-hand side of Eq. (5) to account for the effects of solar reflections and surface emissivity and obtained

$$\bar{I}(\nu)=[\bar{\epsilon}(\nu)B(\nu,T_s)+R_{\text{sun}}(\nu,\theta)\bar{\rho}(\nu)]\tau(\nu,p_s)+I_a(\nu), \quad (8)$$

where $\bar{\epsilon}(\nu)$ and $\bar{\rho}(\nu)$ are the directional spectral surface emissivity and reflectivity in the clear (i.e., horizontally homogeneous) parts of the surface in the four consecutive fields of view. $R_{\text{sun}}(\nu,\theta)$ is the solar irradiance at the surface of the Earth and can be expressed as

$$R_{\text{sun}}(\nu,\theta)=B[\nu,T_{\text{sun}}]\tau_a(\nu,\theta)\cos\theta, \quad (9)$$

where T_{sun} is the brightness temperature of the sun, θ the angle between the sun rays and the local vertical and $\tau_a(\nu,\theta)$ the transmittance of the entire atmosphere along the path traveled by the solar flux in the direction θ. $I_a(\nu)$ is the atmospheric spectral radiance defined as

$$I_a(\nu)=\int_{\ln p_s}^{\ln \bar{p}} B[\nu,T(p)]\frac{\partial\tau(\nu,p)}{\partial \ln p}d\ln p. \quad (10)$$

The true surface temperature T_s can be obtained from Eq. (8) provided $\bar{\epsilon}(\nu)$ and $\bar{\rho}(\nu)$ are known. Shaw (1970) used three channels in the 3.7 μm region to determine T_s, $\bar{\epsilon}$ and $\bar{\rho}$. We have followed the approach suggested by Shaw and found the solution of the resulting system of three linear equations to be stable and straightforward as shown in Section 4.

2) THE 11 μm CHANNEL

In the 11 μm region the effects of solar reflection are small and can be neglected. Thus, Eq. (8) becomes

$$\bar{I}(\nu)=\bar{\epsilon}(\nu)B(\nu,T_s)\tau^{(n)}(\nu,P_s)+\int_{\ln p_s}^{\ln \bar{p}} B[\nu,T(p)]\frac{\partial\tau^{(n)}(\nu,p)}{\partial \ln p}d\ln p, \quad (11)$$

where $\bar{\epsilon}(\nu)$ is the surface emissivity, $T(p)$ the recovered clear-column atmospheric temperature profile and $\tau^{(n)}(\nu,p)$ the atmospheric transmittance corresponding to the recovered distribution of water vapor $q^{(n)}_{H_2O}(p)$. In order to determine the true surface temperature from this single channel we have assumed that $\bar{\epsilon}(900)=1$. This is a reasonable assumption for the ocean surface, but not for land where $\bar{\epsilon}(900)$ can be lower than unity.

In general, by comparing the advantages of the 3.7 and 11 μm regions for sounding the surface temperature we found the 3.7 μm channels to be more useful because of the possibility of eliminating the errors introduced by variations in the surface emissivity and solar reflections and because the surface temperatures derived from the 3.7 μm region have the added advantage of being less dependent on errors in measurement and on uncertainties in the corresponding atmosphere attenuation. For these reason we have selected the 3.7 μm channels to recover all the surface temperature values illustrated in Section 4.

d. Amounts and heights of multiple cloud layers

The evaluation of the amounts and heights of clouds cannot be carried out without specifying their radiative transfer properties. In this paper each of the three cloud layers is assumed to behave like a blackbody at the local ambient temperature. The determination of the corresponding amounts N^1, N^2 and N^3 and heights p_c^1, p_c^2 and p_c^3 requires the solution of a system of six equations of the form

$$\bar{I}(\nu_j)-\tilde{I}(\nu_j)=\sum_{l=1}^{3} N^l G^l(\nu_j,p_c^l) \quad (13)$$

for $\nu_j=2187$, 2203, 2222, 726, 744 and 773 cm^{-1}, where $G^l(\nu_j,p_c^l)$ is given in Part II as the radiance obscured by a black layer of clouds at pressure level p_c^l.

The numerical solution of Eq. (13) can be tedious, but it is possible to uncouple the system of six nonlinear equations and reduce the problem to the solution of a set of just two equations (details of this method will be published in a separate paper). In principle, the approach is similar to that of the single cloud layer described in Section 6 of Chahine (1974), and the solution is accomplished in two steps: the cloud-tops pressure levels p_c^l are computed by minimization techniques and then the cloud amounts are evaluated directly by linear methods.

4. Experimental results

The results from three successful runs of the aircraft are discussed in this section. Each run corresponds to a different range of sun angles and different clouds and weather conditions. The accuracy of the recovered clear-column parameters is illustrated in Figs. 1, 2 and 3. Each figure shows a complete set of results on the same horizontal scale. This format enables us to demonstrate the consistency of the various results and allows us to correlate the various atmospheric parameters with each other.

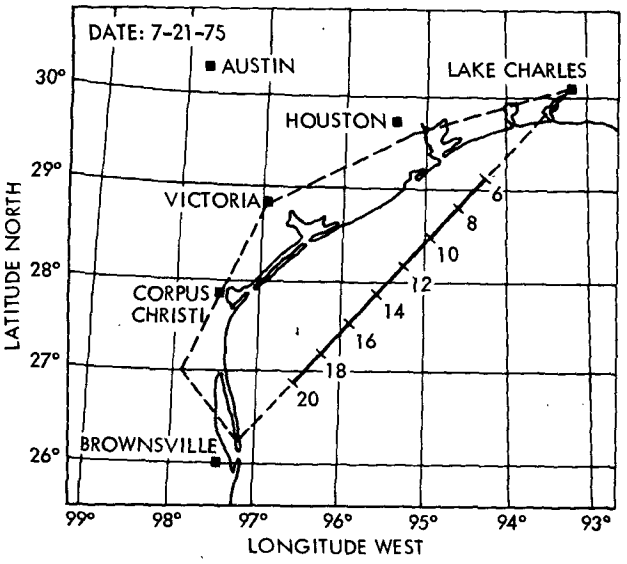

FIG. 1a. Flight path and location of stations for run in Fig. 1b.

a. Figure 1

Fig. 1a shows the flight path for the afternoon flight between Lake Charles and Brownsville. Although measurements were taken along the entire path, the results shown in Fig. 1b only cover the range between station 6 and 20 only. Data measured outside this flight range were discarded because the aircraft did not reach a stable altitude until station 4, and beyond station 20 the aircraft was in a maneuvering mode.

The true surface temperature T_s shown in the lowest block in Fig. 1b is derived from the 3.7 μm channels. The results agree well with the values of bucket temperature obtained from the U. S. Navy catalogs[2] for the same data ($\pm$1 day), time ($\pm$2 h) and location ($\pm$25 km). The sea surface temperature is uniform along the entire path except near station 20 where we notice a dip of 2 K as a result of the vertical convection cell associated with the storm system encountered in that region. The decrease in the value of the surface temperature at station 20 is real and is directly related to the position of the storm. It can be correlated with the sudden decrease in the value of the water vapor mixing ratio at the same station.

The clear-column atmospheric temperature profiles were recovered at six pressure levels between the surface and the aircraft. Typical variations of $T(p)$ are shown at four pressure levels and compared with the corresponding values from the 1800 radiosonde profile measured at Lake Charles. The sudden dip in value of the temperature near station 17 at 400 mb is difficult to explain, but perhaps it could be due to the presence of small amounts of clouds in the vicinity of the aircraft height.

[2] Private communication, Captain C. R. Ward, Fleet Numerical Weather Central, Monterey, Calif.

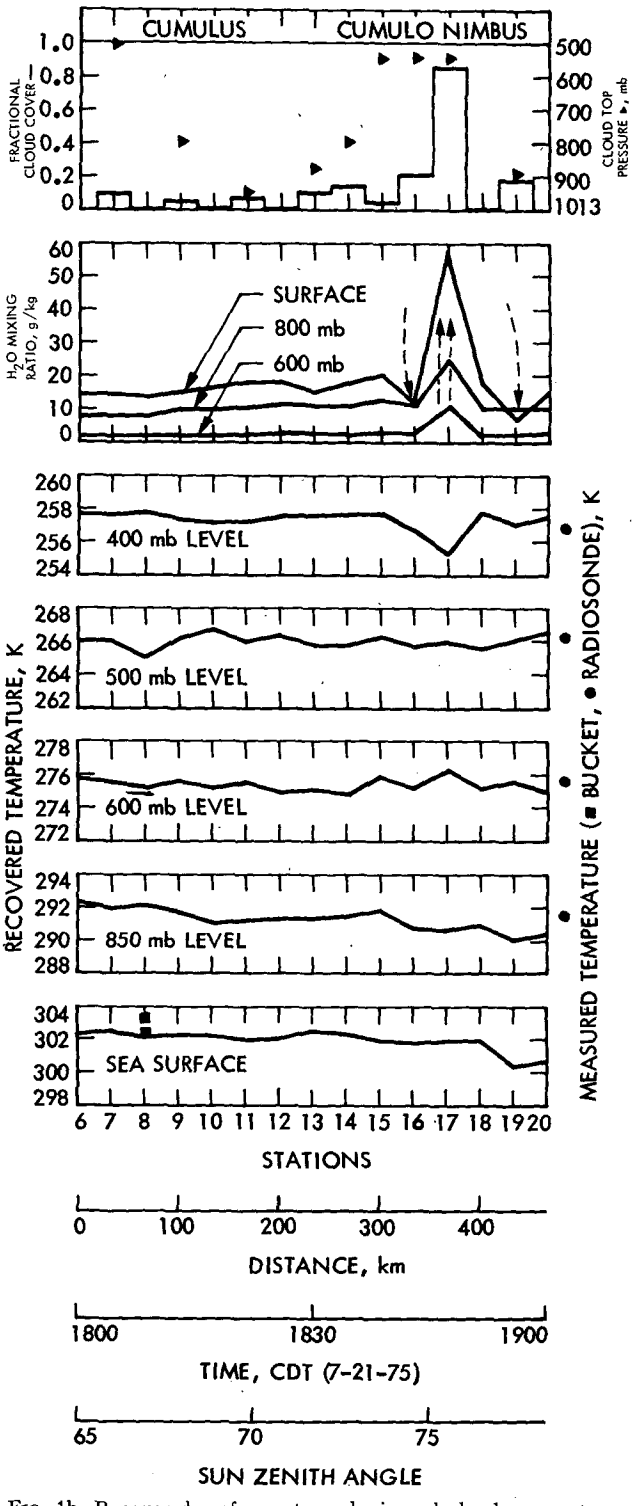

FIG. 1b. Recovered surface, atmospheric and cloud parameters. See text in Section 4a for more details.

The clear-column water vapor mixing ratio corresponding to three pressure levels is shown near the top of Fig. 1b. The mixing ratio is constant from the start until station 16, just before the storm. Between

stations 16 and 19 the distribution of water vapor clearly shows the presence of vertical convection cells which normally accompany the formation of cumulus clouds. We notice warm and humid air ascending at station 17 with cold and dry air descending at stations 16 and 19. The effect of this cell on the sea surface temperature at station 19 has been discussed earlier in this section.

The distribution of the fractional cloud covers and the mean cloud-top pressure levels of the uppermost cloud layer is shown at the top of Fig. 1. Identification of the types of clouds and estimation of their heights were made by visual observations during the flight. In addition, a 35 mm camera, mounted in the instrument package, recorded the cloud amounts on regular commercial films. After analyzing the data we found that the agreement between the fractional cloud covers recovered from the instrument infrared detectors and the amounts appearing in the photographs is excellent for thick clouds and, as expected, poor for thin haze layers. Furthermore, we found the computed cloud-top heights to agree to within ± 300 m with the values estimated during the flight. We observed that the horizontal distribution of the water vapor near the surface offers an unmistakable clue to the identification of convective types of clouds.

b. Figure 2

The results shown in Fig. 2 correspond to an early morning flight with sunrise beginning near station 2 of Fig. 2a. In the lowest block of Fig. 2b we see that the recovered sea surface temperature is uniform between stations 4 and 22, but beyond station 22 the sea surface temperature begins to decrease with increasing depth of the Gulf. Agreement between the recovered true surface temperature and the bucket temperature is excellent at all sun angles and in the presence of different types and amounts of clouds. In the shore area between stations 24 and 27, we observe that the surface temperature is cooler than the ocean surface temperature, as expected during early morning hours. Further inland we notice that T_s increases rapidly as the earth's surface begins to warm up from 0800 to 0900. Quantitative comparisons over land between the recovered surface temperature and the actual surface temperature are not possible because of the difficulty of obtaining direct measurements of the average surface temperature for the specific fields of view of the sounder.

The clear-column atmospheric temperature distribution $T(p)$ is shown at four pressure levels above

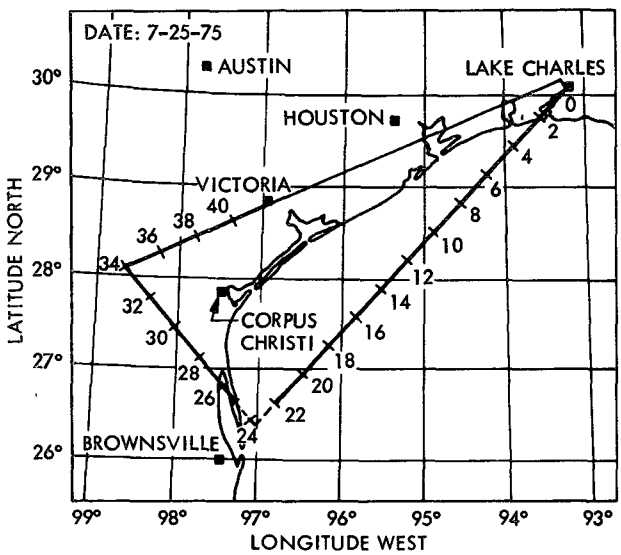

FIG. 2a. Flight path and location of stations of the morning run described in Fig. 2b.

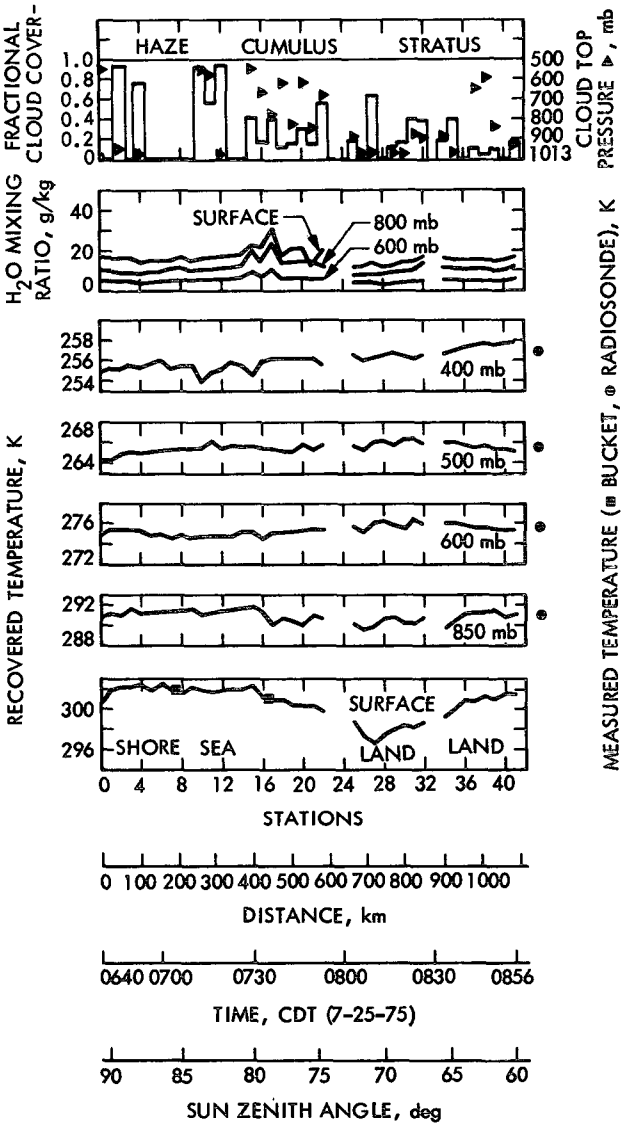

FIG. 2b. Recovered surface, atmospheric and cloud parameters for a morning run. See text in Section 4b for more details.

the surface. We notice that fluctuations in the horizontal distribution of $T(p)$ are within the noise limits of ± 1 K, except for the case of the 400 mb level, just below the aircraft.

The distribution of the water vapor mixing ratio in this run is similar to the case of Fig. 1. We observe again here that cumulus clouds are accompanied by vertical convection cells, as indicated by the water vapor distribution, while in the cases of haze or stratus clouds no such cells appear in the results.

c. Figure 3

Variations of the solar zenith angle for this afternoon flight ranged between 45° near Lake Charles and 65° at Victoria near the end of the flight. The recovered sea surface temperature is uniform and agrees well with the corresponding bucket values and the surface temperature of the shore is warmer for the late afternoon hours.

The measurements obtained at station 18 are an example of a case where the radiances measured over all four fields of view were equal in value. This could be due to the presence of a uniform cloud cover or to the absence of any clouds in all four fields of view. In the former case, the data cannot be analyzed by the present approach. To resolve possible ambiguities we recover the apparent temperature profile (obtained without correction for cloud effects) from the 4.3 μm channels and test to find if this profile satisfies the 15 μm channels. In the case of station 18 the test was negative. We concluded from this that the fields of view must be covered by a uniform layer of thin clouds. To verify this conclusion we analyzed the first field of view of station 18 jointly with the last three fields of view of station 17, and indeed determined that 18% of the first field of view of station 18

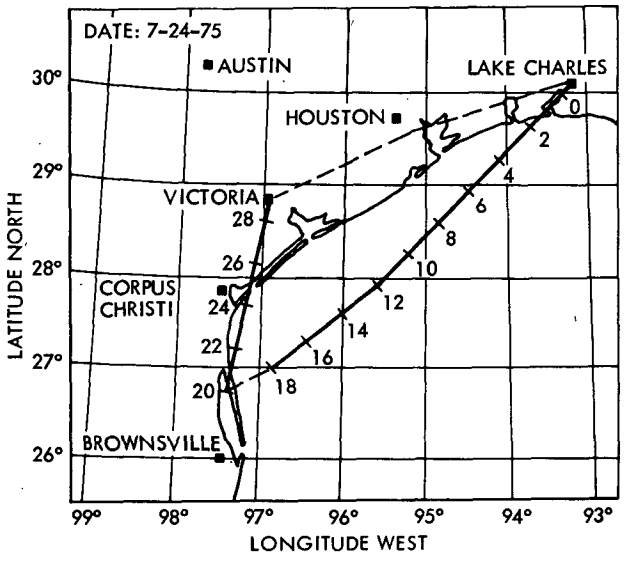

FIG. 3a. Flight path and location of stations of the afternoon run described in Fig. 3b.

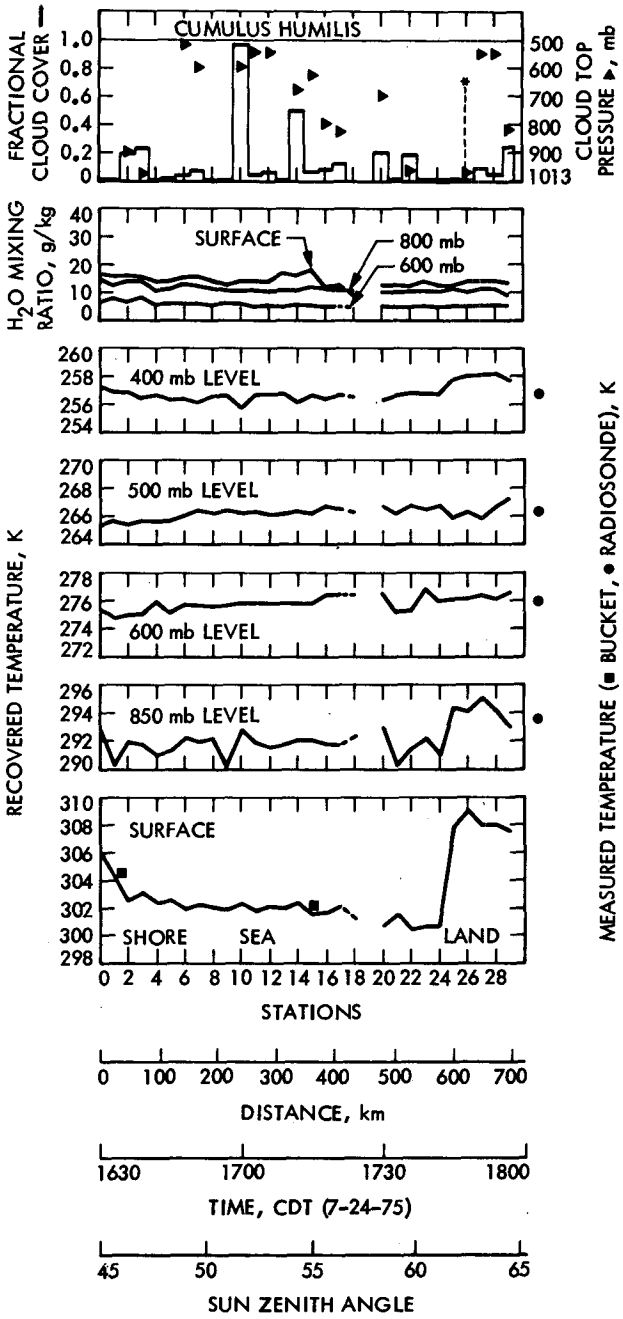

FIG. 3b. Recovered surface, atmospheric and cloud parameters for an afternoon run. See text in Section 4c for more details.

is covered by clouds. It is interesting to note that this is the only case of redundant data encountered in the entire flight test program.

The recovered clear-column atmospheric temperature profile is compared in Fig. 3 with the radiosonde profile measured at Victoria. We observe several large fluctuations in $T(p)$ particularly when crossing over the western shore near station 24.

The recovered clear-column water vapor mixing ratio is very uniform along the entire flight path and gives no indication of convective activity. This be-

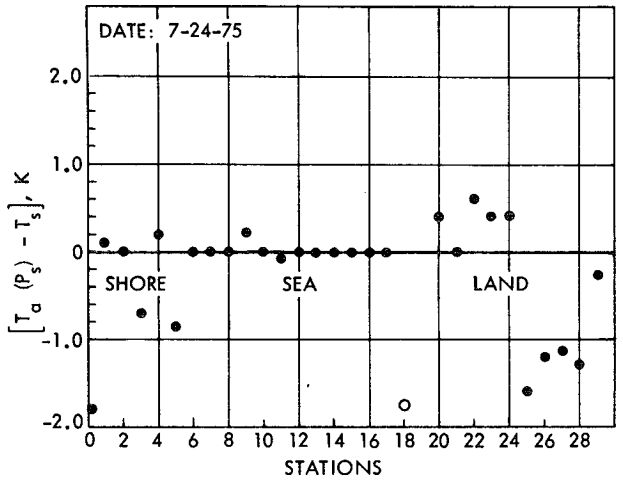

FIG. 4. Comparison between the air temperature at the surface and the true surface temperature for run described in Fig. 3b. See text in Section 4d for details.

havior agrees with the type of fair weather clouds observed during the flight.

In comparing the computed fractional cloud cover at station 26 with the accompanying photograph we noticed that our computations indicated the presence of 70% clouds near the surface at 975±25 mb, while the photographs distinctly showed clear fields of view with a bay (Copano Bay, fed by the Aransas River) covering most of the corresponding surface elements. This result is not unexpected in view of our assumption of black clouds since the water is cooler than its surroundings and cannot be distinguished from a black cloud close to the surface. In general it is always difficult to recover the amount or height of clouds on the basis of infrared observations alone when the clouds are near the surface.

d. Figure 4

In Fig. 4 we compare the air temperature at the surface $T_a(p_s)$ with the true skin surface temperatures T_s derived according to Section 3c. We define the air temperature at the surface as atmospheric temperature at the bottom of the lowest atmospheric slab, obtained according to Section 3a. The subscript a is added here for emphasis only. The results shown in Fig. 4 are for the run discussed in Fig. 3, and they show a very good agreement between $T_a(p_s)$ and T_s over the Gulf. This agreement is a direct consequence of the high level of humidity near the surface during this time of the year. The observed differences over land are due in part to variations in the surface emissivity and to the use of linear interpolation in recovering the clear-column atmospheric temperature profile.

5. Conclusion

The accuracy of the recovered sea surface temperature was emphasized here as a proof of the capability of the cloud-filtering method for two reasons: 1) because the effects of clouds on the upwelling energy from the surface is a maximum and 2) because of the availability of surface truth data. We selected the month of July for the experiment because the sea surface temperature of the Gulf of Mexico is uniform during this month, and thus any deficiency in the cloud filtering method would be much more noticeable against this uniform background.

The main purpose of the three parts of this study has been to develop and to verify experimentally a cloud filtering method for infrared remote sensing of the earth's atmosphere as well as the atmospheres of other planets. The methods applied here to the aircraft experiment are general and can be extended to the case of observations from satellite orbits.

Acknowledgments. We wish to express our thanks to Professor Charles S. Cox of the Scripps Institute of Oceanography, University of California at San Diego, for introducing our work to the North Pacific Experiment (NORPAX) Program and for his assistance in planning the aircraft flight experiment over the area of the Gulf of Mexico.

This paper presents the results of one phase of research carried out at the Jet Propulsion Laboratory, California Institute of Technology, and was supported in part by the National Aeronautics and Space Administration under Contract NAS 7-100 and by the National Science Foundation, Office of the International Decade of Ocean Explorations, and the Office of Naval Research in support of the NORPAX Program, under NSF Grant AG505.

REFERENCES

Aumann, H. H., and M. T. Chahine, 1976: An infrared multidetector spectrometer for remote sensing of temperature profiles in the presence of clouds. *Appl. Opt.*, **15** (in press).

Chahine, M. T., 1968: Determination of the temperature profile in an atmosphere from its outgoing radiance. *J. Opt. Soc. Amer.*, **58**, 1634–1637.

——, 1970: Inverse problems in radiative transfer: Determination of atmospheric parameters. *J. Atmos. Sci.*, **27**, 960–967.

——, 1972: A general relaxation method for inverse solution of the full radiative transfer equation. *J. Atmos. Sci.*, **29**, 741–747.

——, 1974: Remote sensing of cloudy atmospheres. I. The single cloud layer. *J. Atmos. Sci.*, **31**, 233–243.

——, 1976: Remote sensing of cloudy atmospheres. II. Multiple cloud formations. *J. Atmos. Sci.*, **34**, 744–757.

Jastrow, R., and M. Halem, 1973: Accuracy and coverage of temperature data derived from IR radiometer on the NOAA 2 satellite. *J. Atmos. Sci.*, **30**, 958–964.

McClatchey, R. A., W. S. Benedict, S. A. Clough, D. E. Burch, R. F. Calfee, K. Fox, L. S. Rothman and J. S. Garing, 1973: AFCRL atmospheric absorption line parameters compilation. AFCRL Environ. Res. Pap. No. 434, 78 pp.

Shaw, J. H., 1970: Determination of the earth's surface temperature from remote spectral radiance observations near 2600 cm^{-1}. *J. Atmos. Sci.*, **27**, 950–959.